Invited Paper

Crystal Gamma-ray Detectors for High Energy Physics *

Ren-yuan Zhu

California Institute of Technology
Pasadena, CA 91125, USA

ABSTRACT

This report reviews the design characteristics of crystal γ-ray detectors for high energy physics. The unique physics capability of these detectors is the result of their excellent energy resolution, uniform hermetic coverage and fine granularity. To maintain crystal's resolution *in situ* radiation hardness is a principle requirement. The performance of various heavy crystal scintillators is discussed. A technical approach to solve radiation damage problem by optical bleaching *in situ* is elaborated.

Keywords: high-energy physics, particle physics, crystal, scintillator, calorimeter, detector

1 INTRODUCTION

Total absorption shower counters made of inorganic scintillating crystals have been known for decades for their superb energy resolution and detection efficiency. In high energy physics, large arrays of scintillating crystals have been assembled for precision measurement of the energy and angle of photons and electrons. The discovery potential of crystal γ-ray detector was first demonstrated by the Crystal Ball detector[1] through its study of radiative transitions and decays of the Charmonium family (Figure 1[2]). Over the last decade, following the Crystal Ball and CUSB[3] experiments, larger crystal detectors have been constructed, and their use has been a key factor in the successful physics programs of the L3 experiment at LEP,[4] of the CLEO II at CESR[5] and of the Crystal Barrel at LEAR.[6] Similar crystal detectors also have been designed and are under development for the next generation of high energy physics experiments aimed at the study of CP violation. These include KTeV at Fermilab,[7] the BaBar at SLAC[8] and BELLE at KEK.[9]

In addition, a large sector of the high-energy physics community has designed and studied crystal detectors containing 10^4 to more than 10^5 elements, planning to use them for multi-TeV hadron colliders, including the late Superconducting SuperCollider (SSC) in the U.S.[10,11] and the Large Hadronic Collider (LHC) at CERN in Europe.[12,13] Although some of these crystal detector designs[10,11,13] are no longer under consideration for use in an experiment, this development led to significant advances in our understanding of the physics capabilities of these detectors and the crystal detector technology. At the time of this writing, a crystal detector is actively being considered as an option for the CMS electromagnetic calorimeter at the LHC.

The unique physics capability of a crystal detector is the result of its excellent energy resolution, uniform hermetic

*Work supported in part by U.S. Department of Energy Grant No. DE-FG03-92-ER40701.

0-8194-1629-0/94/$6.00

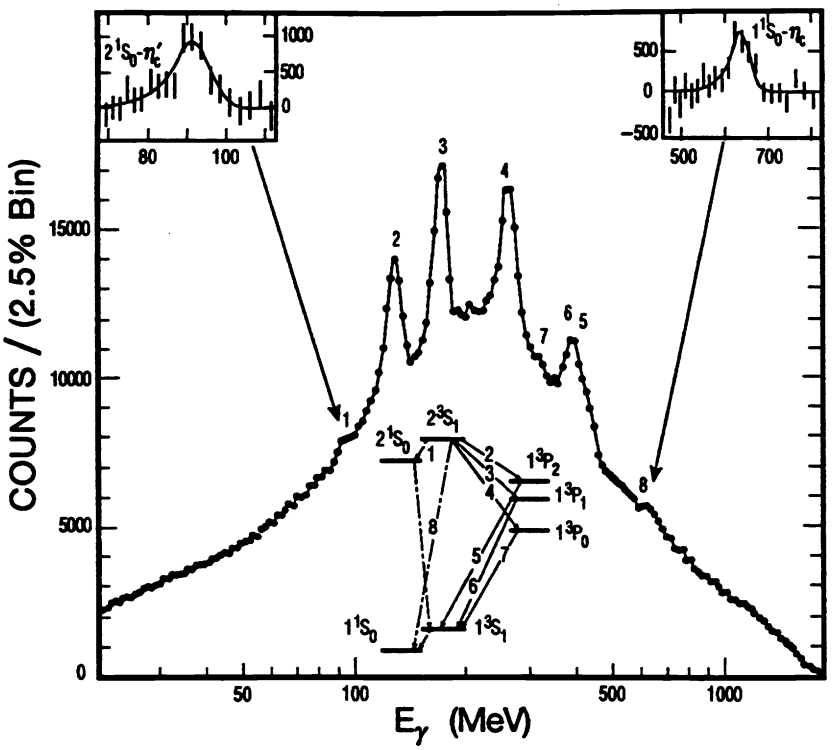

Figure 1: An inclusive photon spectrum measured at the ψ' (3686) by the Crystal Ball experiment at SLAC.[2] Almost all of the principal radiative transitions of the charmonium system are observed simultaneously. The upper inserts show the background subtracted signal from η_c (2980) and $\eta_{c'}$ (3590) states.

coverage, fine granularity, and clean electron and photon identification. All above led to the best efficiency (and signal/background ratio) for the reconstruction of multi-lepton, lepton-photon and multi-photon invariant masses, as well as clean separation of electrons from jets and single hadrons. A well-designed crystal detector is ideal for detecting multi-photon final states containing resonances, such as π^0, η, η', or yet-to-be-discovered high-mass particles such as the Higgs in the intermediate mass range between 80 and 170 GeV, as shown in Figure 2.[14]

In order to maintain crystal's excellent resolution *in situ*, the detector must be resistant to radiation damage caused by large electromagnetic and/or hadronic energy deposition. For experiments to be operated at multi-TeV hadron colliders, very high speed (triggering within the typical beam-crossing time of 25 ns) and radiation resistance up to the 10 Mrad range are among the principal design requirements.

In this report, the main properties of commonly used inorganic heavy crystal scintillators (Section 2) and parameters of the major crystal detectors (Section 3) are described. The achievable performance of crystal detectors and the contributing factors to the resolution are discussed (Section 4). The effect of radiation damage and a technical approach to solve radiation damage problem by optical bleaching *in situ* is elaborated (Section 5).

2 INORGANIC CRYSTAL SCINTILLATORS

The choice of crystal for a γ-ray detector in high energy physics is governed by its material properties (density, melting point, breaking stress, machinability and hygroscopicity), shower containment (radiation length, X_0, and Moliere radius, R_M), scintillation properties (light frequency, light yield, decay speed and temperature dependence), and radiation hardness. Table 1 lists the basic properties of commonly used heavy crystal scintillators

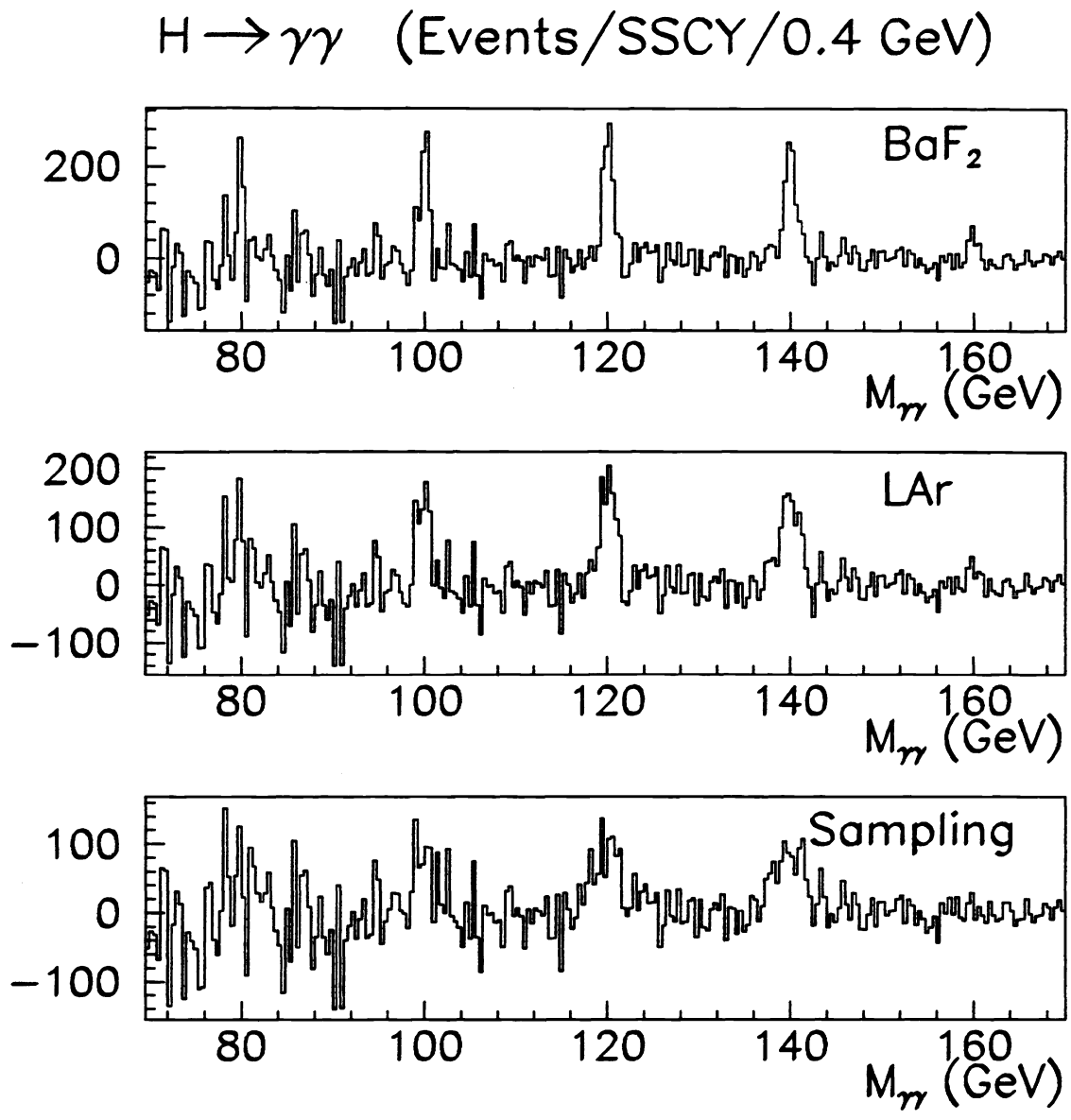

Figure 2: Invariant $\gamma\gamma$ mass spectra predicted for the production of Higgs particles of 80, 100, 120, 140 and 160 GeV, accumulated with 10 fb^{-1} at SSC. The spectra are shown with background subtracted statistically. The mass spectra are given for three energy resolutions corresponding to a BaF_2 crystal detector $(2/\sqrt{E} \oplus 0.5)\%$, a liquid argon (LAr)detector $(7.5/\sqrt{E} \oplus 0.5)\%$ and a sampling detector $(15/\sqrt{E} \oplus 1.0)\%$.

in high energy physics: NaI(Tl),[15] CsI(Tl),[16] undoped CsI,[17–19] BaF_2,[20,21] CeF_3,[22,23] and BGO ($Bi_4Ge_3O_{12}$).[15] Except for CeF_3, these crystals are commercially available in large quantities. The expected price per cm^3 listed in the table corresponds to typical quotations for an order of more than 10^6 cm^3.

Figure 3 (left) shows scintillation pulse of CeF_3, CsI, BaF_2, BGO and CsI(Tl). The very fast scintillation of CeF_3, CsI and BaF_2 is clearly seen in the figure. Figure 3 (right) shows the number of photoelectrons per MeV energy deposition as a function of integration time. For both measurements, a Hamamatsu R2959 PMT was used. All samples used are about 1" × 1" in dimension.

The advantage of NaI(Tl) is high light yield and an emission well-matched to bialkali cathodes of photomultiplier (PMT). However, its hygroscopicity makes it difficult to be handled. Tl doped CsI also has high light yield with an emission well-matched to silicon photodiodes (PD). Its plasticity and mechanical robustness are advantage,

Table 1: Properties of Some Crysatl Scintillators

	NaI(Tl)	CsI(Tl)	Pure CsI	BaF_2	CeF_3	BGO
Density (g cm^{-3})	3.67	4.51	4.51	4.89	6.16	7.13
Melting Point (°C)	651	621	621	1280	1460	1050
Radiation Length (cm)	2.59	1.85	1.85	2.06	1.68	1.12
Moliere Radius (cm)	4.8	3.5	3.5	3.39	2.63	2.33
Interaction Length (cm)	41.4	37.0	37.0	29.9	26.2	21.8
Refractive Index[a]	1.85	1.79	1.95	1.50	1.62	2.15
Hygroscopic	Yes	slightly	slightly	No	No	No
Luminescence[b] (nm)	410	520	420	300	340	480
			310	220	300	
Decay Time[b] (ns)	230	1000	35	630	30	300
			6	0.9	9	
Relative Light Output[b,c]	100	45	4	20	3.5	8
			3	4	3.5	
Price ($/cc)	1–2	2	2.5	2.5	3[d]	7

a At the wavelength of the emission maximum.

b Top line: slow component, bottom line: fast component.

c Measured with a PMT with a bialkali cathode.

d Expected mass-produced price, now in the R&D stage.

while its slightly hygroscopicity requires a careful surface treatment. Undoped CsI has fast scintillation with an emission matched to bialkali cathodes. Its scintillation light has –0.6%/°C temperature dependence.[17] The fast component of BaF_2 is the fastest scintillator and is temperature independent.[20] CeF_3 is a relatively new scintillator[22] with fast scintillation emission similar to pure CsI and is nearly temperature independent.[23] BGO has very high density and short X_0 and R_M with emission matched to silicon photodiodes. It is not hygroscopic and easy to be handled.

In addition to the crystals listed in Table 1, three other heavy crystals have recently been studied. $PbWO_4$ (lead tungstate),[24] PbF_2[25] and Ce-doped lutetium oxyorthosilicate ($Lu_2(SiO_4)O$ or LSO; i.e. $Lu_{2(1-x)}Ce_{2x}(SiO_4)O$.[26] $PbWO_4$ is a very dense (8.28 g cm^{-3}) material with the shortest radiation length (0.85 cm) and Moliere radius (2.2 cm). Its scintillation light is peaked at 440 and 530 nm[24] with a decay time of 10 and 40 ns. The main shortcoming of this material is its low light yield (10-15 photoelectrons/MeV measured with a bialkali photocathode) and strong temperature dependence of the scintillation light (–1.9%/°C). It is now under study by the CMS collaboration at CERN as an alternative to CeF_3, in their consideration of a crystal detector option.

PbF_2 is another dense material (7.77 g cm^{-3}, X_0 = 0.93 cm R_M = 2.21 cm) but it is not a scintillator in its common form. Attempts to dope PbF_2 or to grow orthorhombic structure[27] to make it scintillate have not been successful. It thus does not really belong in this section – it has to be used as a Cherenkov radiator – but it is mentioned because of the substantial work that has been carried out to make it a low cost scintillator.

LSO is also dense (7.41 g cm^{-3}, X_0 = 1.14 cm, R_M = 2.3 cm; similar in these respects to BGO). Its scintillation light is peaked at 440 nm (a good match to bialkali cathodes), with a decay time of 40 ns. Its light output is 75% of NaI(Tl). Test have also shown that it is radiation hard to 100 Mrad.[28] The main obstacles to large scale use of LSO, however, are a very high melting point (> 2,000°C) and very high price (~100 $/cc for crystals produced during R&D). A similar material is Ce doped GSO, $Gd_2(SiO_4)O$,[29] which has similar desirable properties and practical drawbacks.

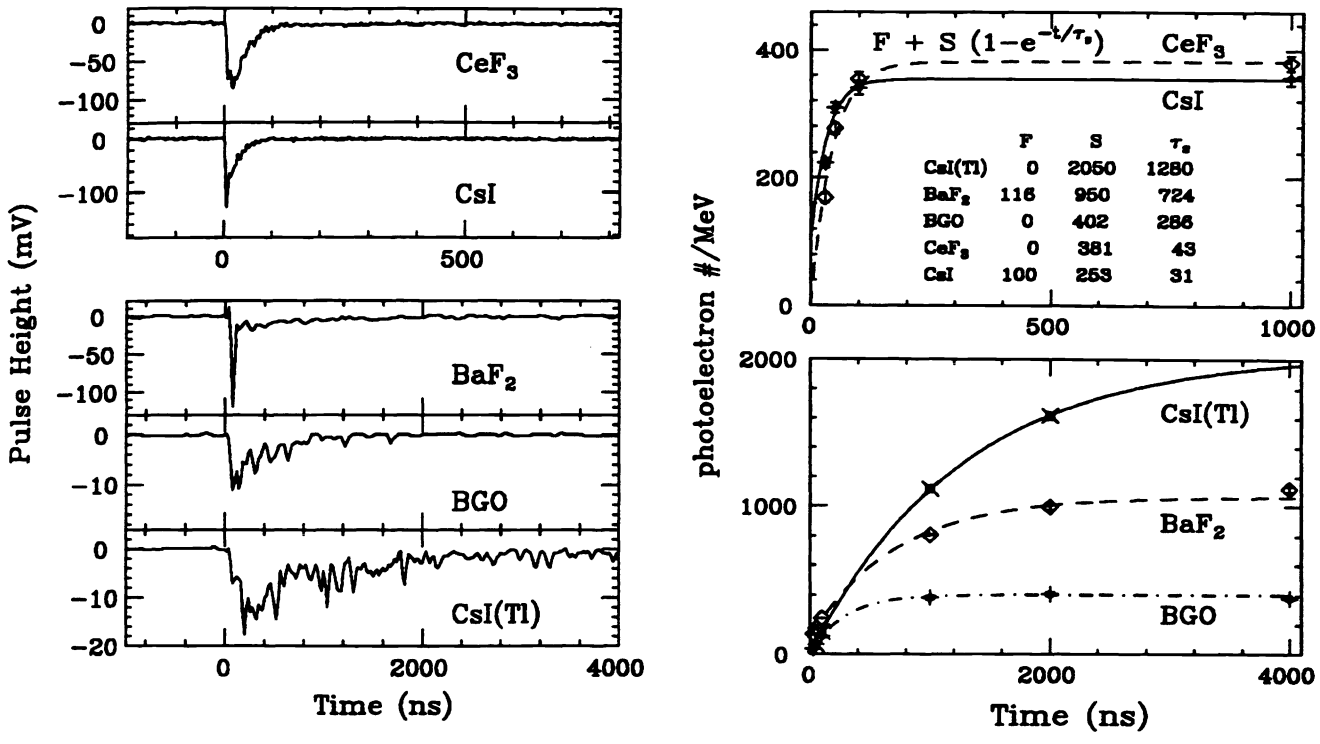

Figure 3: Scintillation pulse (left) of ^{137}Cs γ-ray, recorded with an HP 54111D digital scope, and number of photoelectron per MeV as a function of integration time (right), for CeF_3, CsI, BaF_2, BGO and CsI(Tl) crystals coupled to an R2059 PMT.

3 CRYSTAL γ-RAY DETECTORS

Tables 2 and 3 list parameters of crystal detector projects of the recent past (Crystal Ball), present (L3, CLEO II, Crystal Barrel) and future (KTeV, BaBar, BELLE, CMS) in high energy physics. The parameters a_0 and a_1 represent contributions to the energy resolution (at 1 GeV) from electrical noise and photoelectron statistics, respectively (See Equation 1). Figure 4 shows the crystal arrangement of the L3 BGO detector as an example. The BaF_2 detector design for the GEM experiment[11] at the SSC, and the CeF_3 detector design for the L3P experiment at the LHC[13] are included for completeness.

The details of the design of each crystal detector are governed by its physics goals, which are usually related to precision measurements of photons and electrons.[30] At low energies (below a few hundred MeV), the large light yields (photoelectrons/MeV) are needed to achieve good energy resolution. These requirements have been met by the Crystal Ball using NaI, and by CLEO II, Crystal Barrel, BaBar and BELLE using CsI(Tl). At high energies (above few tens GeV), the energy resolution of a crystal detector is dominated by systematics. The CMS, L3P and the GEM projects have enough crystal length to achieve a systematic accuracy of less than 0.5%. In the case of KTeV, the crystal length (27 X_0) also is dictated by the requirement that the energy resolution function have a sufficiently small tail, such that an absolute systematic uncertainty level of 0.02% in the γ energy-scale can be attained, following extensive calibration.[7]

The inner radius of a crystal detector is a tradeoff between the required performance and cost. A larger radius would provide better 2γ separation, and thus higher efficiency of π^0 reconstruction and/or rejection, but with a larger volume of crystals and hence increased cost. The lateral segmentation is a tradeoff between position resolution, which improves with finer segmentation, and the number of readout channels. Longitudinal segmen-

Table 2: Crystal Detector Parameters

Experiment	C. Ball	L3	CLEO II	C. Barrel	KTeV
Accelerator	SPEAR	LEP	CESR	LEAR	FNAL
Inner Radius (m)	0.254	0.55	1.0	0.27	-
B-Field (Tesla)	-	0.5	1.5	1.5	-
Number of Crystals	672	11,400	7,800	1,400	3,300
Crystal Type	NaI(Tl)	BGO	CsI(Tl)	CsI(Tl)	CsI
Crystal Length (X_0)	16	22	16	16	27
Crystal Volume (m^3)	1	1.5	7	1	2
Light Output (p.e./MeV)	350	1,400	5,000	2,000	40
Photosensor	PMT	Si PD	Si PD	WS[a]+Si PD	PMT
Gain of Photosensor	Large	1	1	1	4,000
Noise/Channel (MeV)	0.05	0.8	0.5	0.2	Small
Dynamic Range	10^4	10^5	10^4	10^4	10^4
a_0[b] (%)	0.02	0.3	0.2	0.06	<0.1
a_1[c] (%)	0.2	0.1	0.05	0.07	0.5

a Wavelength Shifter.

b Noise contribution to the energy resolution (at 1 GeV).

c Photoelectron statistics contribution to the energy resolution (at 1 GeV).

Table 3: Parameters of Recently Designed Crystal Detectors

	BaBar	BELLE	CMS	(GEM)	(L3P)
	PEP-II	KEK	LHC	SSC	LHC
Inner Raddius (m)	1.0	1.25	1.3	0.8	2.9
B-Field (Tesla)	1.5	1.0	4.0	0.8	2.0
Number of Crystals	10,000	8,900	43,200	15,000	129,600
Crystal Type	CsI(Tl)	CsI(Tl)	CeF_3	BaF_2	CeF_3
Crystal Length (X_0)	18	16	25	24.5	23.2
Crystal Volume (m^3)	10	10	26	11	~50
Light Output (p.e./MeV)	5,000	5,000	300	30	50
Photosensor	Si PD	Si PD	Si PD	VPT[a]	VPT[a]
Gain of Photosensor	1	1	1	12	10
Noise/Channel (MeV)	0.03	0.03	20	3	20
Dynamic Range	10^4	10^4	10^5	10^5	10^5
a_0[b] (%)	0.01	0.01	6	1	6
a_1[c] (%)	0.03	0.03	0.2	0.6	0.5

a Vacuum photo tube.

b Noise contribution to the energy resolution (at 1 GeV).

c Photoelectron statistics contribution to the energy resolution (at 1 GeV).

tation of the crystals would provide an angular measurement for high energy isolated photons.[21,31] This would

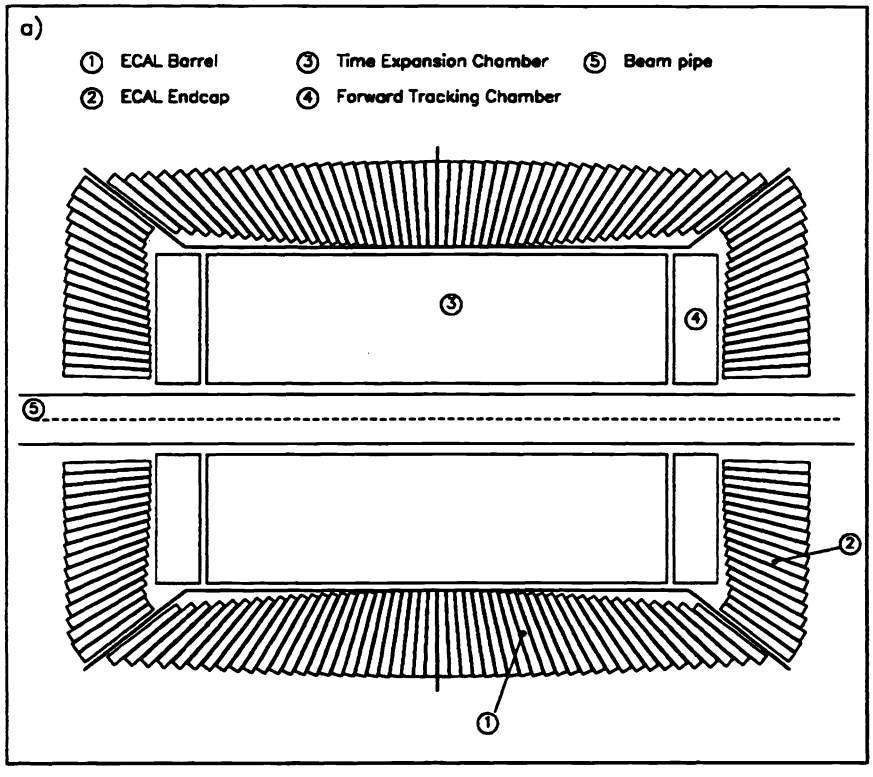

Figure 4: A longitudinal cut through the L3 BGO crystal detector.

be advantageous at future hadron colliders to determine the vertex of the photon pair at high luminosities in the 10^{34} cm^{-2} s^{-1} range, where multiple minimum-bias events will overlap with the event of interest at every bunch crossing, but at the price of a much larger number of crystal pieces and readout channels.

The choice of photosensor and its gain are governed by the magnetic field, the crystal type (e.g. by the wavelength of the scintillation light) and by the energy-equivalent noise per channel. Operation in a magnetic field excludes the possibility of using most multistage vacuum phototubes. The photosensor choices include silicon photodiodes, vacuum diodes or triodes (VPT),[32] or proximity-focused few stage grid mesh tubes recently developed by Hammamatsu.[33]

4 ENERGY RESOLUTION OF CRYSTAL γ-RAY DETECTORS

In high energy physics, the energy resolution of a crystal γ-ray detector can be parametrized as:

$$(\frac{\Delta E}{E})^2 = (\frac{\mathbf{a_0}}{E})^2 + (\frac{\mathbf{a_1}}{\sqrt{E}})^2 + \mathbf{b}^2 \quad (1)$$

where $\mathbf{a_0}$ is the contribution from electronic noise, summed over the readout channels within a few Moliere radii around the center of the lateral shower distribution, and $\mathbf{a_1}$ is the contribution from the photoelectron statistics, related to the photon yield of the crystal and the fraction of crystal's end face covered by the photosensor. The systematic, or constant, term b has three main contributions:

$$\mathbf{b}^2 = \mathbf{b_G}^2 + \mathbf{b_C}^2 + \mathbf{b_n}^2. \quad (2)$$

Here b_G represents the geometry effect, including shower leakage from the back, side, and front (albedo), and absorption of part of the shower in the inactive material in front of and between cells. The typical lower limit of b_G is 0.3 to 0.4%, and it may become larger at both lower and upper ends of the energy range of interest. b_C represents the inter-calibration error between crystals. Depending on the calibration method(s) used, the typical lower limit on this term is 0.3%. b_n is the contribution from non-uniformities in the crystal response, caused by intrinsic attenuation length, reflector efficiency variations or radiation-induced non-uniformities. This term contributes to the resolution because the shower length and width of electromagnetic shower fluctuate for articles of the same incident energy.

At low energy, the dominant contributions to the energy resolution are the electronic noise term (a_0/E). The sampling term ($a_1/\sqrt{E}$) dominates in the range of medium to high energies, up to the high energy limit where the systematic term (b) becomes dominant. Tables 2 and 3 list values of the coefficients a_0 and a_1 for various crystal calorimeter systems. Each table entry is calculated analytically using the energy-equivalent noise (in MeV) per readout channel, the light output per unit energy deposited (photoelectrons/MeV), and assuming a summation of 3 × 3 channels to form an electromagnetic cluster representing an electron or photon.

The electronic noise also determines the lower limit of the *energy reach*, as well as the resolution and photon identification efficiency at the low energy end. For a given type of crystal, this term is determined by the choice of photosensor. In the case of a silicon photodiode, the noise is controlled by the diode's area and thickness, and the fraction of the rear crystal face covered. A larger collection area corresponds to a larger signal per unit energy, but also a larger electronic noise, caused by the larger capacitance and leakage current.

The resolution at the high energy end is limited by systematics. Once a sufficiently precise intercalibration

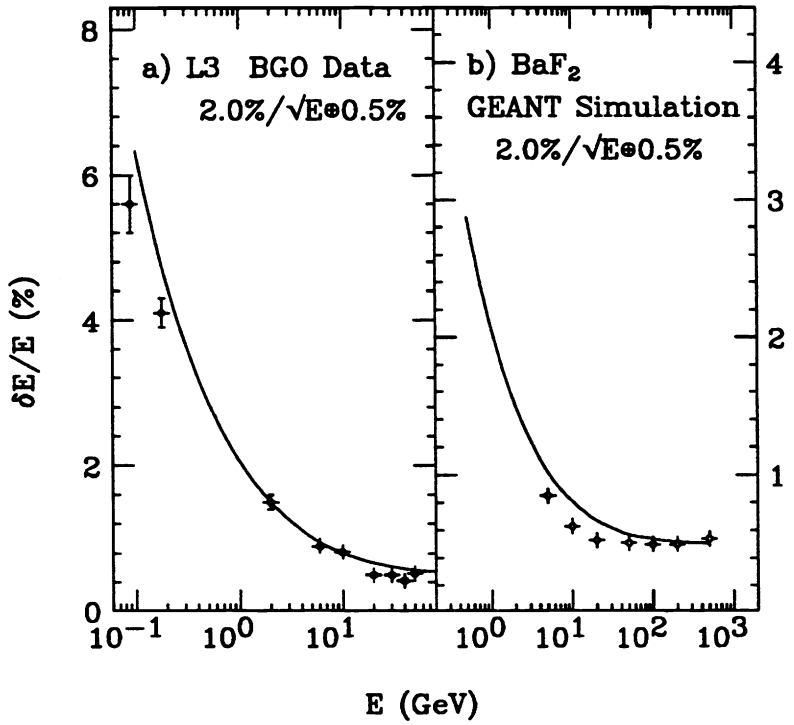

Figure 5: Energy Resolutions of (a) a 4000 crystal half-barrel of the L3 BGO detector, measured in test beams at the CERN SPS (2 – 50 GeV), the LEP injector (180 MeV extracted beam) and CESR (100 MeV),[4] and (b) a BaF_2 detector, simulated with the parameters listed in Table 4. the solid curves represent a simple parametrization: $2\%/\sqrt{E} \oplus 0.5\%$.

Table 4: Energy Resolution (%) of a BaF_2 Calorimeter

E (GeV)	5	10	20	50	100	200	500
Electronic Noise	0.4	0.2	0.1	0.04	0.02	0.01	0.004
Photoelectrons	0.2	0.14	0.1	0.063	0.045	0.03	0.02
Leakage (b_G)	0.60	0.43	0.32	0.30	0.30	0.30	0.36
Intercalibration (b_C)	0.40	0.40	0.40	0.40	0.40	0.40	0.40
Total	0.85	0.63	0.53	0.51	0.50	0.50	0.54

(b_C) and a uniform light response (b_n) are achieved the ultimate energy resolution of a crystal calorimeter is determined by the shower leakage and absorption term (b_G). This term can be reliably estimated by a "realistic" GEANT[34] simulation which includes an accurate geometrical representation of the calorimeter support structures, the crystal wrapping material and air gaps between crystals. A typical result[21] of this kind of simulation is listed in Table 4 for electrons with different energies (5, 10, 20, 50, 100, 200 and 500 GeV), in terms of σ of the peak, defined as the full width at half maximum (FWHM) divided by 2.35. As shown in the Table, this GEANT simulation predicts a constant term not less than 0.3%. For very high energies, the systematic contribution is somewhat larger, caused by rear leakage because of limited calorimeter length.

Assuming an inter-calibration accuracy of 0.4% and light response uniformity (b_n) is under control, the total expected energy resolution is also listed in Table 4. This resolution can be parametrized as $2\%/\sqrt{E} \oplus 0.5\%$, as shown in Figure 5b. For a comparison, Figure 5a shows the measured energy resolution of 4,000 BGO crystals (one half-barrel) compared to the same parametrization.

5 CRYSTAL RADIATION DAMAGE

All known large crystal scintillators suffer radiation damage[1]. The principal damage phenomenon, observed in all mass-produced crystals, is the appearance of absorption bands, caused by color center formation. The absorption bands reduce the transmission of scintillation light through the crystals to the photosensors, and hence the apparent light yield following irradiation. Additional effects observed in some crystals include reduced intrinsic yield of scintillation light, increased fluorescence (afterglow), and phosphorescence (spontaneous light emission over a long period). It is important that a crystal's scintillation mechanism not be damaged and that the radiation-induced phosphorescence does not affect the readout signal. By choosing crystals, these criteria can be met. However, the increased radiation-induced absorption (equivalently: a reduced light attenuation length) changes the light response uniformity, and thus may degrade the energy resolution.

5.1 Crystal light response uniformity

Figure 6[21] shows the GEANT predictions for the energy fraction (top figure) and the intrinsic energy resolution (bottom figure) for a BaF_2 crystal detector, as a function of the light response uniformity. In this simulation, the light response (Y) of the crystal was parametrized as a normalized linear function:

$$Y = Y_{25}\,[1 + \delta(z/25 - 1)] \tag{3}$$

[1] See papers by Y. Dafinei, D. Hitlin, H. Newman, B. Winstein, C. Woody, C. Wuest and R.Y. Zhu, in *Proceedings of the Crystal 2000 International Workshop*.[35]

where Y_{25} represents the light response at the middle (25 cm) of a 50 cm BaF_2 crystal, δ represents the deviation of the light response uniformity, and z is the distance from the small (front) end of a tapered crystal. To maintain a systematic limitation to the intrinsic energy resolution to less than 0.5%, the δ value is required to be less than 5%, and thus a light attenuation length (LAL) of longer than 95 cm. A detailed study using many different functional forms of the light response non-uniformity, in addition to a linear dependence, confirmed this conclusion quantitatively.[36]

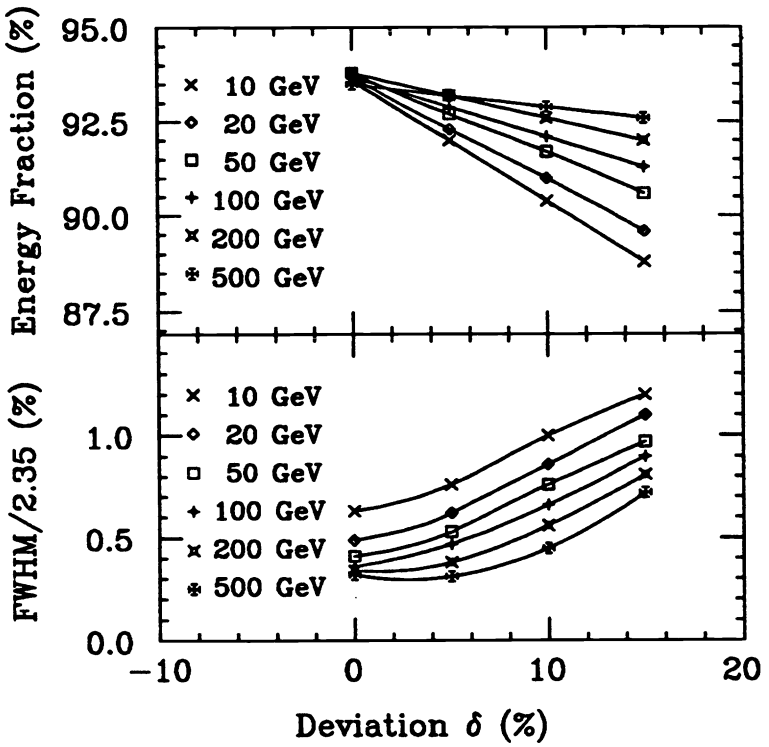

Figure 6: The relative mean energy fraction and the energy resolution for electromagnetic clusters of 3 × 3 crystals as a function of light response uniformity, derived with a GEANT simulation.[21] See Equation 3 in the text for the definition of parameter δ.

Light response uniformity can be achieved by using special wrapping or coating techniques. For a tapered crystal with its 6 faces polished, there are two counterbalancing factors which affect the light uniformity over the crystal length: the light attenuation (both bulk attenuation and losses at each reflection) and an "optical focusing" effect. The optical focusing effect can be understood in terms of Liouville's theorem: as the crystal gets larger and a bundle of light rays thus is allowed to expand, the individual rays within the bundle tend to become more parallel to the long axis of the crystal. While light attenuation causes a decrease of the response with increasing distance from the photosensor, the optical focusing effect leads to higher light collection efficiency and thus increasing response with distance. For a 24 cm BGO crystal, the second factor dominates: a strong increase of the light response (up to a factor of 2.4) at the small end compared to the large end was observed for L3 crystals which had all sides well-polished.[4]

In general, uniform light response has been obtained by treating at least part of the crystal surface to avoid total internal reflection that continues over many bounces – effectively "trapping" part of the light in the crystal – and to instead scatter the light diffusely, randomizing the direction of light rays within the crystal. Common techniques are (1) depolishing the lateral crystal faces in a nonuniform and carefully controlled manner (Crystal

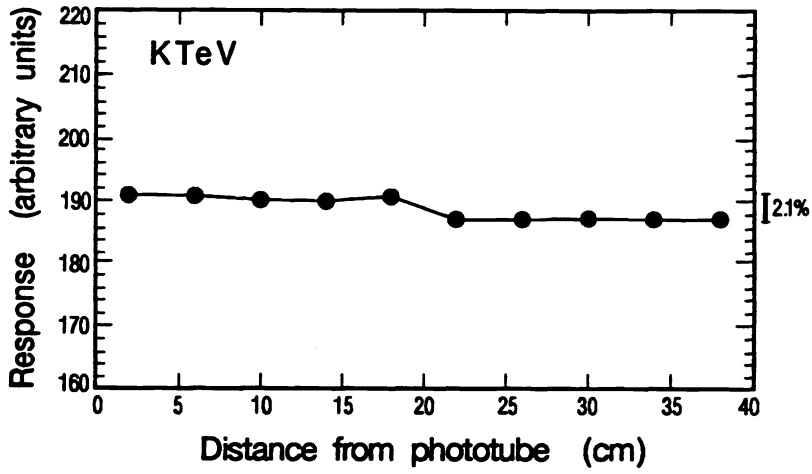

Figure 7: The light response of a 40 cm CsI crystal with teflon wrapping is shown as a function of the distance from the PMT.[7] The overall nonuniformity is around 2.1%.

Ball),[37] (2) coating all surfaces of the crystals with a highly reflective diffuse reflector, such as a 40-50 μm thick coating NE560 white paint NE560 (L3 BGO calorimeter),[4] or (3) teflon or aluminized mylar wrapping (KTeV CsI calorimeter).[7] Figure 7 shows the light response uniformity of a 40 cm CsI crystal with teflon wrapping measured by KTeV.[7] A deviation of 2.1% over the crystal length is achieved.

5.2 Radiation damage phenomena

The radiation-induced color center formation may destroy the light response uniformity because of the reduced light attenuation length. The colr center is usually related to impurities and/or structural defects in the crystals. The impurities may be present as substitutional or interstitial trace element atoms in the lattice, or they may occur as molecular ions, or microscopic color center complexes containing many atoms. Based on the extensive literature on high purity silicon crystals, and the specific studies of BGO and BaF_2 scintillators, it is known that the impurities also may lead to macroscopic structures which have a high density of trace-element rich color center complexes clustered together. These structures form inclusions which are visible under a low power microscopic, and in some cases to the naked eye.

A study of (1) the trace element content and distribution in the crystals, (2) the quality of the crystal structure, and (3) the density and structure of the inclusions in a series of crystal samples was carried out for BGO in 1981—85,[38–40] and for BaF_2 from 1988—93.[41,42,21] This data was cross-correlated with the degree of radiation damage in a series of doped and undoped crystal samples. This led to greatly improved processing technology for both types of crystals. As a result of the improved control of raw materials, crystal growth and annealing methods, crystals with greater radiation resistance were produced, especially for BaF_2 . Studies of the radiation damage problem for pure and doped CsI,[43,18] CeF_3[44,23] and $PbWO_4$[45] are also underway.

Studies of BGO indicate that key impurities at the sub-ppm level may cause severe damage.[39,46] Figure 8[39] shows the relative light output as a function of time after irradiation with a 2.5 krad dose, for BGO samples doped with different dopants.This data led to the conclusion that impurities in the BGO crystal can be categorized in three classes: (1) "harmful" impurities which cause permanent or severe damage (Cr, Mn, Fe and Pb), (2) "less harmful" impurities which cause some damage (Co, Ga, Mg and Ni) (3) "harmless" impurities which cause no discernible damage (Al, Ca, Cu and Si) at the typical trace impurity levels found in standard-quality crystals. The figure also illustrates that different doped and undoped BGO crystal samples recover at different rates, with characteristic recovery times ranging from hours to weeks.

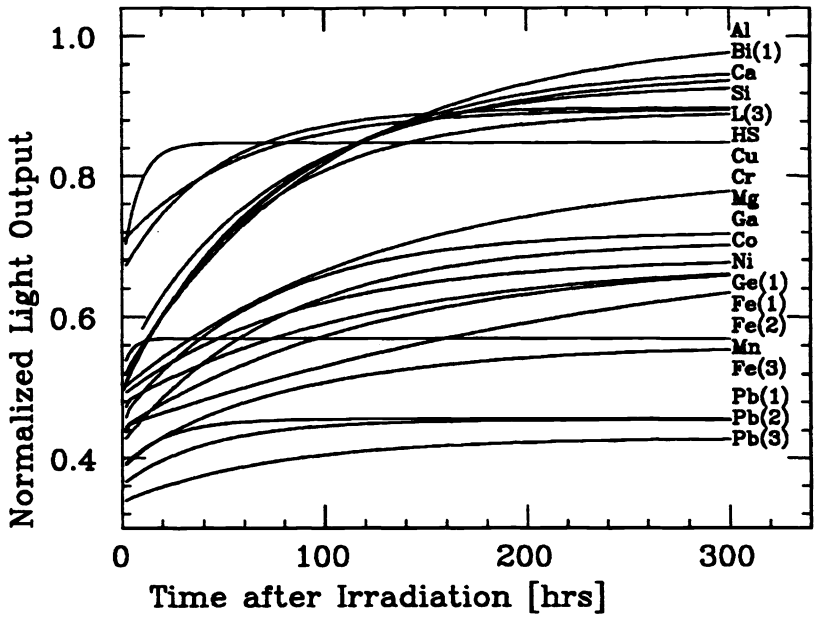

Figure 8: Relative pulse height as a function of the time after irradiation with a 2.5 krad dose, for BGO crystals doped with different dopants.[39]

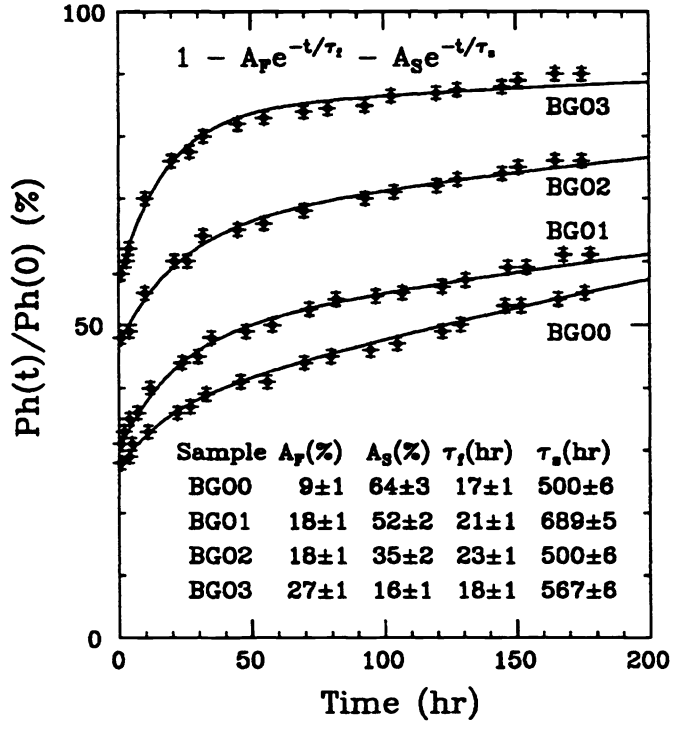

Figure 9: Relative pulse height as a function of the time after a 2.5 krad dose is shown for for four BGO crystals doped with different levels of europium: 0, 5, 10 and 100 ppm by weight for BGO0, BGO1, BGO2, and BGO3 respectively.[40]

For BGO crystals, it was discovered that europium doping improved the radiation resistance by accelerating the

recovery from the damage at room temperature. Figure 9[40] shows the relative pulse height as a function of time after a radiation dose of 2.5 krad from a ^{137}Cs γ-ray source for four BGO crystals doped with different levels of europium: 0, 5, 10 and 100 ppm by weight for the samples labeled BGO0, BGO1, BGO2 and BGO3 in the figure. The damage level is shown in terms of the parameters A_F and A_S from a fit to a function of 1 - A_F e^{-t/τ_f} - A_S e^{-t/τ_s}. It is clear that the damage level ($A_F + A_S$), especially the slow recovery component decreases with increased europium doping. The Eu-doped BGO crystals are used in the rings of crystals in L3's BGO endcaps closest to the beam line, where the dose is higher than the barrel.

The main conclusions from the investigations of radiation damage in BaF_2 crystals are:

- As in BGO, the damage of BaF_2 is caused by the formation of color centers, which introduce a self-absorption of the scintillation light. There is no damage to the scintillation mechanism itself.
- There is no permanent damage in BaF_2 caused by doses from photons, neutrons or other hadrons (such as protons, pions or kaons). At room temperature, the recovery of the damage is extremely slow (characteristic times of many months to years). However, all damage recovers fully after thermal annealing at 500°C in an inert dry atmosphere for three hours. UV light also has been found to be effective in removing the radiation damage.
- The radiation damage of BaF_2 shows clear saturation, in both transmittance and light yield measured by the photosensor, after an initial dose of 100 krad or less. This means that additional doses of Mrads result in no further change in transmittance, once saturation has been reached. The saturation phenomenon indicates that the number of color centers is relatively few, as expected for damage controlled by trace impurities.
- The damage has no dependence on the radiation dose rate.

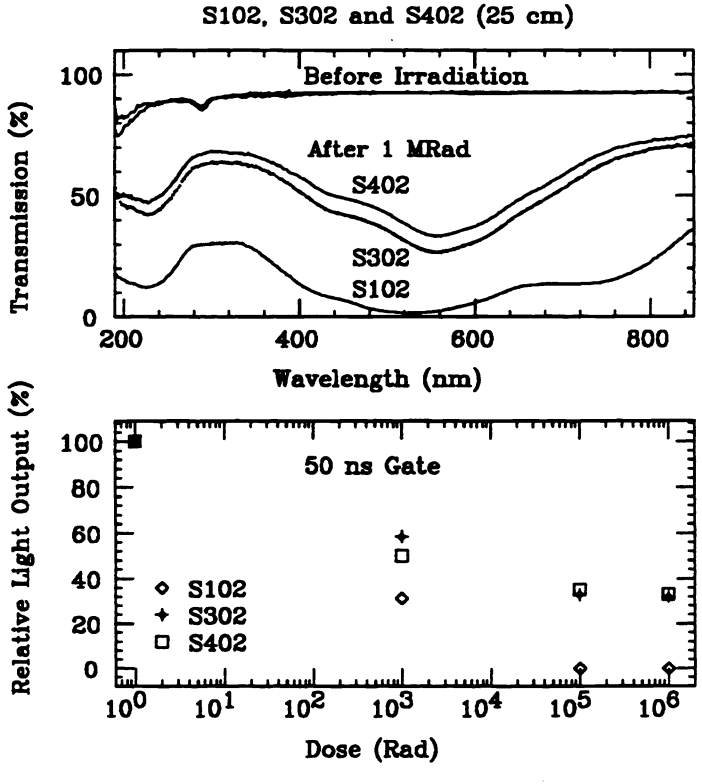

Figure 10: (a) Transmittance and (b) relative light output are shown for three 25 cm BaF_2 crystal produced at SIC in early 1991 (SIC102), early 1992 (SIC302) and July 1992 (SIC402), after a 1 Mrad γ-ray dose.[21]

- The basic radiation damage mechanism is understood. Impurities (such as rare earths),[47,48] defects (inclusions),[49,48] oxygen[49] and OH^- (U and O^- substitutional centers)[50,51] are responsible.

Figure 10[21] shows (a) the transmittance before and after 1 Mrad γ-ray irradiation and (b) the relative light output measured for three 25 cm BaF_2 crystal produced at the Shaghai Institute of Ceramics (SIC) in early 1991 (SIC102), early 1992 (SIC302) and July 1992 (SIC402). The progressive improvement of the quality of production BaF_2 crystals is clearly seen from the figure.

5.3 Optical bleaching *in situ*

The improvement of the intrinsic radiation resistance, by purification of the raw materials and the use of optimized growth and annealing cycles, is a very difficult, time-consuming and expensive process. As shown in Figure 10, the light attenuation length of 25 cm BaF_2 crystals currently produced at SIC and Beijing Glass Research Institute (BGRI), after 1 Mrad of saturated irradiation is 42 cm.[52] This did not meet the GEM specifications (95 cm attenuation length) as of August 1992. A technique for annealing BaF_2 crystals *in situ*, i.e. optical bleaching, was

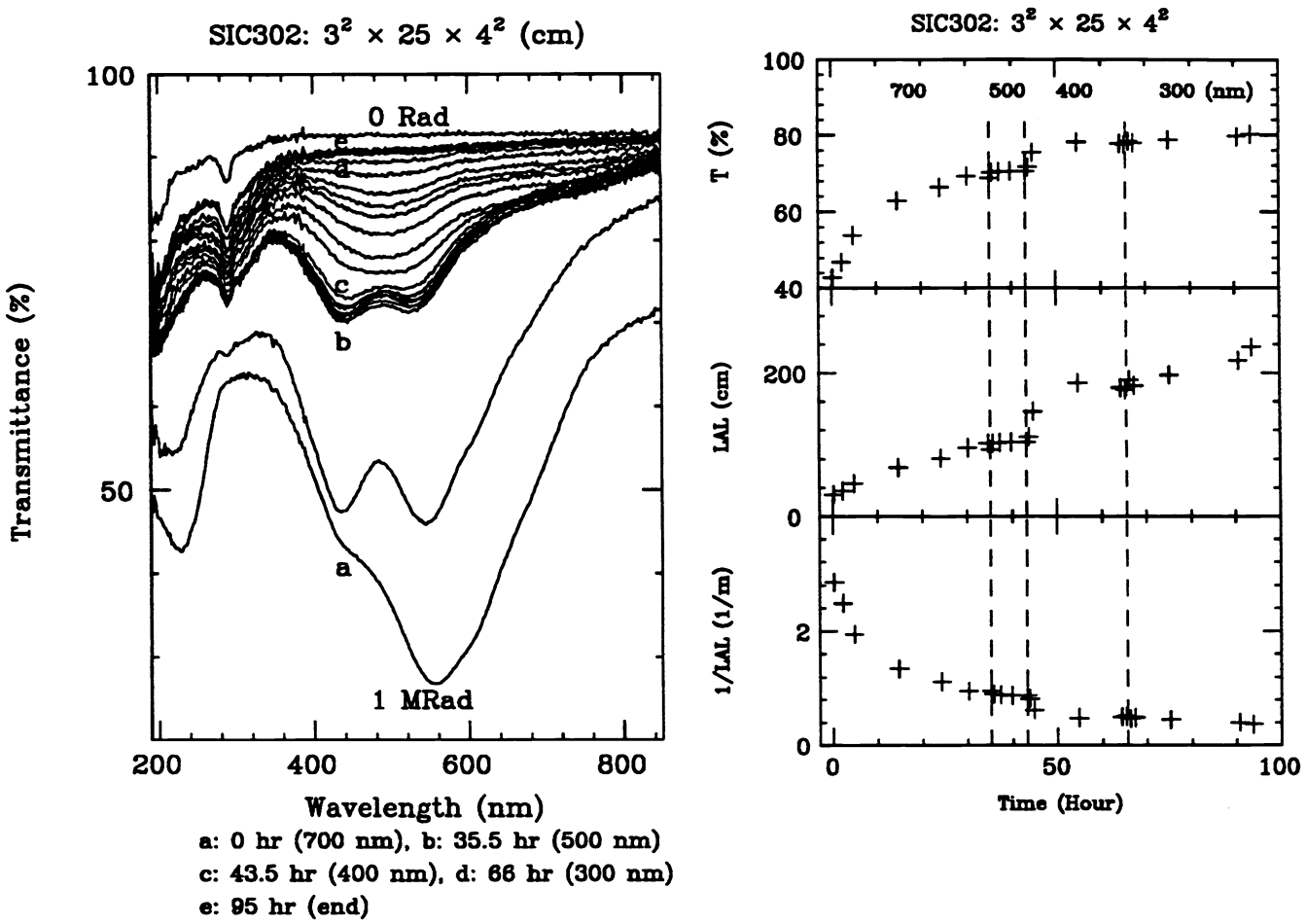

Figure 11: Transmittance as a function of wavelength (left) and transmittance at 220 nm, corresponsing light attenuation length and color center density as a function of time (right) are shown for a 25 cm BaF_2 crystal under optical bleaching with light of different wavelengths.[55]

proposed by a BaF_2 Expert Panel, which was specially organized by the SSC Laboratory to evaluate the radiation damage problem of BaF_2, and assist in setting research directions for the development of BaF_2 crystals to be used at multi-TeV hadron colliders.[53] Following the Panel's recommendations, several independent measurements on optical bleaching were carried out.[54–57,51]

It was found that the optical bleaching with visible light was effective in removing the radiation damage. Studies also were performed to characterize the spectral behavior, required light intensity, and rate of bleaching. The damage effect was found to be annealable with very low light intensities carried over silica fibers,[54] and at wavelengths as long as 700 nm. THe left side of Figure 11 shows the recovery of transmittance of a 25 cm crystal after 1 Mrad irradiation by optical bleaching. The transmittance (T) at 220 nm (BaF_2 fast comonent) and corresponding light attenuation length (LAL) and color center density (1/LAL) are shown in the right side of Figure 11. It was determined[55] that the light intensity required to restore the crystals to a stable light attenuation length of at least 150 cm — well beyond the GEM specifications — to be in the range of mW/cm^2.

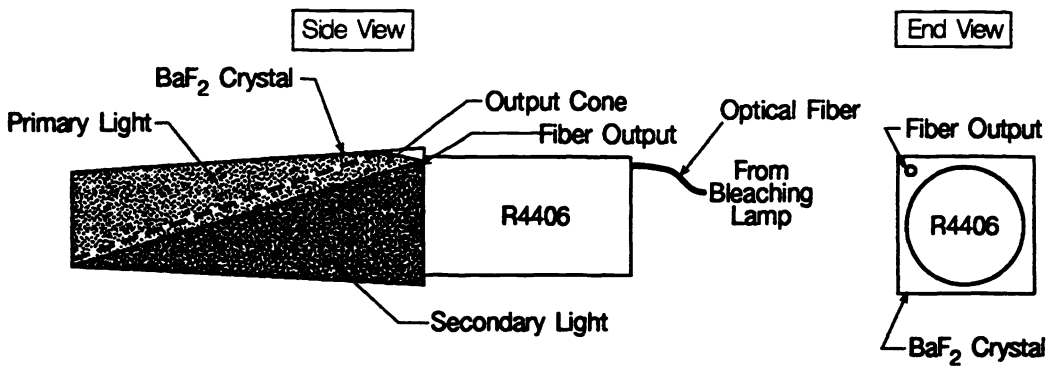

Figure 12: Schematic view of bleaching light propagation in a BaF_2 crystal in the test setup used at Caltech, where light directly from fiber (primary light) has an open angle of 60°, while the reflected light (secondary light) covers the whole volume of the crystal.

Figure 12 shows a practical implementation of optical bleaching through a 2 m long ϕ0.6 mm fiber, in a test setup. The crystal was simultaneously irradiated with a dose of 130 rads/hr, and illuminated with a calibrated bleaching light power through the fiber of 1.6 mW (integrated from 200 to 500 nm) from a 150 W xenon lamp. This modest amount of bleaching light resulted in a stable attenuation length of 170 cm,[21] well in excess of the required value of 95 cm. The large opening angle of the light cone from the fiber (60°), and the reflection of the bleaching light at crystal surface, ensure that the entire crystal is uniformly illuminated. For a large crystal calorimeter, the fiber system could be very similar to the xenon flasher system used to monitor the L3 BGO crystals.[4]

It also has been determined that the color center density in BaF_2 crystals follows a simple dynamical model of color center creation and annihilation.[55] If both the creation and annihilation processes exist at the same time for one kind of color center, the density obeys the equation

$$dD = -aIDdt + (D_{all} - D)\, bRdt \tag{4}$$

where D is the optically bleachable color center density, a is a constant in units of $cm^2\ mW^{-1}\ hr^{-1}$, I is the light intensity in $mW\ cm^{-2}$, D_{all} is the total density of traps related to the optically bleachable color centers in the crystal, b is a constant in units of $krad^{-1}$, R is the radiation dose rate in units of krad hr^{-1}, and t is the time in hours. The solution of Equation 4 is

$$D = D_0 e^{-(aI+bR)t} + \frac{bRD_{all}}{aI+bR}\left[1 - e^{-(aI+bR)t}\right] \tag{5}$$

where D_0 is the initial value of the bleachable color center density. For each value of I and of R, and for one kind of color center, an equilibrium between annihilation and creation will be established at an optical bleachable

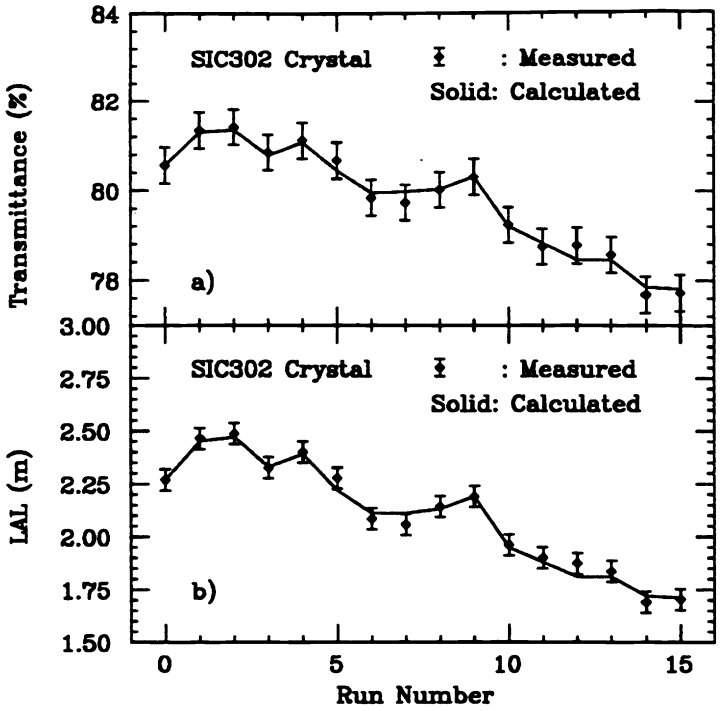

Figure 13: Measured (points) and calculated (solid line) (a) transmittance and (b) light attenuation length (LAL) for a 25 cm BaF_2 crystal in a series of tests with simultaneous ^{60}Co irradiation and 450 nm light illumination.[21]

color center density (D_w) of

$$D_w = \frac{bRD_{all}}{aI + bR} \tag{6}$$

Figure 13[21] shows measured transmittance and corresponding light attenuation length for a series of test runs. The light attenuation length, calculated according to Equation 5 for each specific conditions, is shown as the solid line. The parameters a, b and D_{all} were determined from previous measurements to be: a = 0.68 and 0.95 cm^2 j^{-1} for D < 0.08 and > 0.08 respectively, b = 0.65 $krad^{-1}$ for accumulated dose < 5 krad, and D_{all} = 0.73 m^{-1}. The agreement between the data and the model is very good.

6 CONCLUSION

The high resolution and uniform hermetic coverage of homogeneous crystal γ-ray detectors have given past and present experiments unique physics discovery potential. Over the last two decades, large detectors of this type have achieved resolutions meeting or approaching their design values. To reach and maintain this resolution, radiation hardness and precision inter-calibration *in situ* are among the primary requirements at future multi-TeV hadron colliders. Recent extensive reserach and development has demonstrated that mass-produced crystals of sufficient quality could be obtained, and stable uniform response and the intrinsic resolution could be achieved (through optical bleaching) to meet these requirements. This and recent studies of other scintillating crystals lead us to believe that a precision crystal γ-ray detector could have a key role to play in a wide range of science program, including, but not restricted by, the next generation of hadron colliders.

7 ACKNOWLEDGEMENTS

Many inspiring and interesting discussions with Drs. D. Anderson, G. Chen, G. Gratta, P. LeCoq, P.J. Li, D. Ma, S. Majewski, H. Newman, M. Schneegans, P. Schotanus, R. Sparow, M. Strathman, C. Woody, C. Wuest, D. S. Yan and Z. W. Yin, are greatly appreciated.

8 REFERENCES

[1] M. Oreglia *et al*, *Phys. Rev. D* **25** 2295 (1982).

[2] E. Bloom and C, Peck, *Ann. Rev. Nucl. Part. Sci.* **33** 143-197 (1983).

[3] T. Böringer *et al*, *Phys. Rev. Lett.* **44**: 1111 (1980); G. Mageras *et al*, *Phys. Rev. Lett.* **46**: 1115 (1981).

[4] L3 Collaboration, *Nucl. Instr. and Meth.* **A289** 35 (1990).

[5] Y. Kubota *et al*, *Nucl. Instr. and Meth.* **A320** 66 (1992).

[6] E. Aker *et al*, *Nucl. Instr. and Meth.* **A321** 69 (1992).

[7] K. Arisaka *et al*, *KTeV Design Report*, **FN-580**, January (1992).

[8] *BaBar Letter of Intent*, **SLAC-443**, June (1994).

[9] *BELLE Letter of Intent*, **KEK Report 94-2**, April (1994).

[10] *L* Letter of Intent to the SSC Laboratory*, November (1990).

[11] *GEM Letter of Intent*, **SSCL SR-1184**, November (1991).

[12] *Compact Muon Solenoid Letter of Intent*, CERN/LHCC 92-3, LHCC/I1 (1992).

[13] *L3P Letter of Intent*, CERN/LHCC 92-5, LHCC/I3 (1992).

[14] R.Y. Zhu and H. Yamammoto, **GEM TN-92-126** and **CALT 68-1802** (1992).

[15] Harshaw-QS, *Scintillation Detectors*, (March 1992).

[16] BDH Limited, *BDH Crystran — Monocrystal Products for Optics*, (January 1990).

[17] C. Woody *et al*, *IEEE Trans.* **NS-37** 492 (1990) and **NS-39** 524 (1992).

[18] Z.Y. Wei and R.Y. Zhu, *Nucl. Instr. and Meth.* **A326** 508 (1993).

[19] P. Schotanus, *SCIONIX Internal Report* **93002**, May 1993. **A326** 508 (1993).

[20] P. Schotanus *et al*, *Nucl. Instr. and Meth.* **A238** 564 (1985); M. Kobayashi *et al*, *Nucl. Instr. and Meth.* **A270** 106 (1988).

[21] R.Y. Zhu, *Nucl. Instr. and Meth.* **A340** 442 (1994).

[22] D. Anderson, *IEEE Trans.* **NS-36** 137 (1989); and W. Moses and S. Derenzo, *IEEE Trans.* **NS-36** 173 (1989).

[23] Crystal Clear Collaboration, *Nucl. Instr. and Meth.* **A332** 373 (1993).

[24] M. Kobayashi *et al*, *Nucl. Instr. and Meth.* **A335** 509 (1993).

[25] E. Dally and R. Hofstadter, *Rev. Sci. Instr.* **39** 658 (1968); D. Anderson *et al*, *Nucl. Instr. and Meth.* **A290** 385 (1990); and C. Woody *et al*, *IEEE Trans.* **NS-40** 546 (1993).

[26] C. Melcher and J. Schweitzer, *Nucl. Instr. and Meth.* **A314** 212 (1992) and IEEE Trans. **NS-39** 502 (1992).

[27] D. Anderson *et al*, *Nucl. Instr. and Meth.* **A342** 473 (1994); and C. Wuest *et al*, *talk in Crystal Clear Collaboration Meeting* (December 1993).

[28] M. Kobayashi *et al*, *Nucl. Instr. and Meth.* **A333** 429 (1993).

[29] H. Suzuki, Ph. D. Thesis, Caltech (1994).

[30] G. Gratta, H. Newman and R.Y. Zhu, *Annu. Rev. Nucl. Part. Sci.* **44** 453 (1994).

[31] Clayton *et al*, **CMS TN/92-50** and **IC HEP/93-1** (1992).

[32] Hamamatsu Photonics K.K., *R4406 specification.*

[33] S. Suzuki, *Proposal to Develop a Remote Processed Proximity Focused Phototube*, July (1992).

[34] Brun R *et al*, *GEANT3*, **CERN DD/EE/84-1** (1987).

[35] *Heavy Scintillators for Scientific and Industrial Applications*, Editions Frontieres Volume C58, ed. F. Nataristefani *et al*, September 1992.

[36] Shmakov K, **GEM TN-92-143**, August (1992).

[37] Oreglia M, Ph.D. Thesis, Stanford University, SLAC Report 236 (1980).

[38] M. Kobayashi *et al*, *Nucl. Instr. and Meth.* **A206** 107 (1983); C. Laviron and P. Lecoq, *Nucl. Instr. and Meth.* **A227** 45 (1984); G. Bobbink *et al*, *Nucl. Instr. and Meth.* **A227** 470 (1984); and C. Bieler *et al*, *Nucl. Instr. and Meth.* **A234** 435 (1985).

[39] R.Y. Zhu *et al*, *Nucl. Instr. and Meth.* **A302** 69 (1991).

[40] Z.Y. Wei *et al*, *Nucl. Instr. and Meth.* **A297** 163 (1990).

[41] S. Majewski and D. Anderson, *Nucl. Instr. and Meth.* **A241** 76 (1985); and S. Majewski and M. Bently, *Nucl. Instr. and Meth.* **A260** 373 (1987).

[42] A. Caffreay *et al*, *IEEE Trans.* **NS-33** 230 (1986); M. Murashita *et al*, *Nucl. Instr. and Meth.* **A243** 67 (1986); A. Marakami *et al*, *Nucl. Instr. and Meth.* **A253** 163 (1986) and **A301** 435 (1991); C. Woody *et al*, *IEEE Trans.* **NS-36** 536 (1989) and **NS-39** 123 (1992); and Z. Wei *et al*, *Nucl. Instr. and Meth.* **B61** 61 (1991).

[43] M. Kobayashi and S. Sakuragi, *Nucl. Instr. and Meth.* **A254** 275 (1987); C. Bieler *et al*, *Nucl. Instr. and Meth.* **A234** 435 (1985); H. Grassmann *et al*, *Nucl. Instr. and Meth.* **A228** 323 (1985); S. Schlogl *et al*, *Nucl. Instr. and Meth.* **A242** 89 (1985); D. Hitlin and G. Eigen, in reference[35] p.467.

[44] C. Woody *et al*, **BNL-49866**, submitted to *IEEE Trans. Nucl. Sci.* (1993).

[45] Crystal Clear Collaboration, **CERN-DRDC-93-31** (1993); and C. Woody *et al*, *Phenix Note PX-63* (1993).

[46] T.Q. Zhou *et al*, *Nucl. Instr. and Meth.* **A258** 58 (1987).

[47] G. Chen *et al*, in *Supercollider 4*, ed J. Nonte, Plenum Press, 809 (1992).

[48] M. Strathman, *Report on material chracterization of BaF_2 samples*, (June–August 1992).

[49] P. Li *et al*, in *Supercollider 4*, ed J. Nonte, Plenum Press, 801 (1992); Z. Yin, Talk given in East Asia/Pacific – US Symposium on SSC, (May 1992).

[50] L. Chen *et al*, **GEM TN-92-129** (1992); L. Wang *et al*, *The Optical and Radiation Damage Properties of Barium Fluoride Crystals*, talk presented in Shanghai BaF_2 Workshop, Shanghai, (May 1991).

[51] L. Halliburton *et al*, University of West Virginia Optoelectronics Group Technical Reports, (April–August 1992).

[52] D.A. Ma and R.Y. Zhu, *Nucl. Instr. and Meth.* **A333** 422 (1993).

[53] S. Majewski *et al*, *BaF_2 Expert Panel Report*, (February and August 1992).

[54] S. Stoll, BNL Report, (August 1992).

[55] D. Ma and R.Y. Zhu, *Nucl. Instr. and Meth.* **A332** 113 (1993).

[56] C. Wuest and G. Mauger, LLNL Report, (August 1992).

[57] R. Shang, *Optical Annealing of BaF_2 Crystals with Laser Beam*, (August 1992).